atmosphere

MDPI

Communication

CO_2 Absorption by Solvents Consisting of TMG Protic Ionic Liquids and Ethylene Glycol: The Influence of Hydrogen Bonds

Bohao Lu [1], Yixing Zeng [2,3], Mingzhe Chen [1], Shaoze Zhang [2,3,*] and Dezhong Yang [1,*]

[1] School of Science, China University of Geosciences, Beijing 100083, China; 2119210053@email.cugb.edu.cn (B.L.); 2019220039@email.cugb.edu.cn (M.C.)
[2] National Engineering Research Center of Vacuum Metallurgy, Kunming University of Science and Technology, Kunming 650093, China; zengyx@stu.kust.edu.cn
[3] Engineering Laboratory for Advanced Battery and Materials of Yunnan Province, Kunming University of Science and Technology, Kunming 650093, China
* Correspondence: szzhang@kust.edu.cn (S.Z.); yangdz@cugb.edu.cn (D.Y.)

Abstract: Herein, the absorption of CO_2 by the TMG-based (TMG: 1,1,3,3-tetramethylguanidine) ionic liquids (ILs) and the absorbents formed by TMG ILs and ethylene glycol (EG) is studied. The TMG-based ILs used are formed by TMG and 4-fluorophenol (4-F-PhOH) or carvacrol (Car), and their viscosities are low at 25 °C. The CO_2 uptake capacities of [TMGH][4-F-PhO] and [TMGH][Car] are low (~0.09 mol CO_2/mol IL) at 25 °C and 1.0 atm. However, the mixtures [TMGH][4-F-PhO]-EG and [TMGH][Car]-EG show much higher capacities (~1.0 mol CO_2/mol IL) than those of parent ILs, which is unexpected because of the low CO_2 capacity of EG (0.01 mol CO_2/mol EG) in the same conditions. NMR spectra and theoretical calculations are used to determine the reason for these unexpected absorption behaviors. The spectra and theoretical results show that the strong hydrogen bonds between the $[TMGH]^+$ cation and the phenolate anions make the used TMG-based ILs unreactive to CO_2, resulting in the low CO_2 capacity. In the Ils-EG mixtures, the hydrogen bonds formed between EG and phenolate anions can weaken the $[TMGH]^+$–anion hydrogen bond strength, so ILs-EG mixtures can react with CO_2 and present high CO_2 capacities.

Keywords: carbon dioxide; ionic liquids; hydrogen bonds; absorption; ethylene glycol

Citation: Lu, B.; Zeng, Y.; Chen, M.; Zhang, S.; Yang, D. CO_2 Absorption by Solvents Consisting of TMG Protic Ionic Liquids and Ethylene Glycol: The Influence of Hydrogen Bonds. *Atmosphere* **2024**, *15*, 229. https://doi.org/10.3390/atmos15020229

Academic Editor: Kumar Vikrant

Received: 5 January 2024
Revised: 6 February 2024
Accepted: 8 February 2024
Published: 14 February 2024

1. Introduction

The increasing anthropogenic CO_2 emissions are regarded as the main root of global warming and climate change, which poses a great threat to the environment. Cutting CO_2 emissions has become an urgent issue today and has received substantial attention. A lot of technologies have been designed and applied to reduce CO_2 emissions [1,2]. Among them, carbon capture technology plays a crucial role in curbing carbon emissions. Currently, alkanolamine-based aqueous solutions are widely used as CO_2 capture absorbents to absorb CO_2 in industrial gas streams, which can form carbamate species in the absorption process. Nonetheless, these alkanolamine-based methods suffer serious shortcomings, such as solvent degradation and their high energy cost to regenerate absorbents [3,4]. Therefore, it is also important to develop effective and efficient CO_2 capture methods.

Ionic liquids (ILs) have gained considerable attention because of their fascinating properties, such as extremely low vapor pressure, low flammability, high ionic conductivity, and high thermal stability [5,6]. ILs are usually obtained by combining organic cations like ammonium, imidazolium, and phosphonium; inorganic or organic anions like chloride; and dicyanamide hexafluorophosphate. The characteristics of ILs can be tuned by changing the structures of the component ions and the cation–anion combinations to meet specific applications [7,8], which make them promising alternatives to traditional organic solvents and volatile molecular solvents in many areas of applications.

ILs have also been used as absorbents to capture CO_2 and exhibit promising performance. Functionalized ILs which can chemically capture CO_2 have received a great deal of interest owing to their high CO_2 capture capacities [9–11]. Amino-functionalized ILs, which have amino groups on cations or anions, could absorb CO_2 through the reaction between CO_2 and amino groups by forming carbamate species [12]. Carboxylate-anion-functionalized ILs are also found to be reactive to CO_2. For instance, the carboxylate-based IL 1-ethyl-3-methylimidazolium acetate ([Emim][Ac]) could chemically capture CO_2 through the interactions between CO_2 and *N*-heterocyclic carbene intermediate [13]. Moreover, azolide-based functionalized ILs containing aprotic heterocyclic anions (AHAs) [14–16], such as imidazolide, triazolide, 2-cyano-pyrrolide, and benzimidazolide, have also been developed to capture CO_2. The basicity of azolide anions impacts both CO_2 capacities and absorption enthalpies. Functionalized ILs with phenolic anions and hydroxypyridine anions are also used to absorb CO_2. CO_2 can react with the O atom of phenolic anions by forming carbonate species [17], while CO_2 reacts with both the O and N atoms of hydroxypyridine anions to form carbonate species and carbamate species [18], respectively. In addition, ILs with imide anions are also used for CO_2 capture, and the structures of imide anions greatly affect the CO_2 chemisorption behaviors of ILs [19].

Protic ILs (PILs) have been developed as well for CO_2 capture because the method for synthesizing them is relatively simple. They can be easily obtained just by mixing organic bases with organic/inorganic acids. The organic bases used to prepare PILs are usually superbases, such as 1,8-diazabicyclo-[5,4,0]undec-7-ene (DBU), 1,5-diazabicyclo [4.3.0]non-5-ene (DBN), 1,3,4,6,7,8-hexahydro-1-methyl-2*H*-pyrimido[1,2-α]-pyrimidine (MTBD), and 1,1,3,3-tetramethylguanidine (TMG). To date, the superbase-derived PILs have been widely explored to capture CO_2, such as [MTBDH][Im](Im: imidazolide), [DBUH][Im], [DBNH][Im], [DBUH][Triz](Triz: 1,2,4-triazolide), [DBUH][PhO], and [TMGH][2-OP] [20–24]. Amine-based PILs are used to capture CO_2 as well, such as [DMPDAH][Ac] ((3-dimethylamino)-1-propylammonium acetate), [DMEDAH][Pyr] (*N*,*N*-dimethylethylenediammonium pyrazolide), [DMEDAH][Im], and [MEAH][Im] (monoethanolammonium imidazolide) [25–31].

Herein, we investigate the CO_2 capture by phenol-based PILs, namely [TMGH][4-F-PhO] (4-F-PhO: 4-fluorophenolate) and [TMGH][Car] (Car: carvacrolate). The CO_2 capture by the solvents formed by the ILs and ethylene glycol (EG) is also studied. The CO_2 capacities of [TMGH][4-F-PhO] and [TMGH][Car] are low at 25 °C and 1.0 atm. However, the mixtures [TMGH][4-F-PhO]-EG and [TMGH][Car]-EG exhibit a much higher capacity than [TMGH][4-F-PhO] and [TMGH][Car], although the CO_2 capacities of both the ILs and EG are low in the same conditions. The results from NMR, FTIR, and theoretical calculations indicate that the CO_2 absorption behaviors greatly depend on the hydrogen bond strength in the solvents.

2. Materials and Methods

2.1. Materials and Characterizations

TMG (98%) and EG (99.5%) were supplied by J&K Scientific Ltd. (Beijing, China). Carvacrol (98%) and 4-fluorophenol (99%) were obtained from Innochem (Beijing, China). EG and TMG were dried using 4 Å molecular sieve. CO_2 (99.995%) was supplied by Beijing ZG Special Gases Sci. and Tech. Co., Ltd. (Beijing, China).

FTIR spectra were acquired on a Perkin–Elmer frontier spectrometer (PerkinElmer Corp., Waltham, MA, USA) equipped with an attenuated total reflection (ATR) accessory. ^{1}H NMR (600 MHz) and ^{13}C NMR (151 MHz) spectra were obtained on a Bruker spectrometer (Bruker Biospin, Karlsruhe, Germany), using DMSO-d_6 as the internal reference. The viscosities of solvents were determined on an Anton Paar MCR92 (Anton Paar, Graz, Austria) viscometer at 25 °C. The melting points of ILs and IL-EG mixtures were measured by differential scanning calorimetry (DSC) using a Mettler Toledo DSC1 (Mettler Toledo, Greifensee, Switzerland) instrument at a heating rate of 10 °C/min under N_2 atmosphere.

2.2. Synthesis of ILs and IL-EG Mixtures

In a round-bottom flask (10 mL), 4-F-PhOH or Car was mixed with TMG at an equimolar ratio. Then, the solution was stirred for about 2 h at 40 °C to obtain ILs.

In a round-bottom flask (25 mL), the IL ([TMGH][4-F-PhO] or [TMGH][Car]) was mixed with EG at desired molar ratios, and the IL-EG absorbents were obtained by stirring the mixtures for about 2 h at room temperature.

2.3. Absorption of CO_2

The procedures of CO_2 absorption can be found in our previous work [27].

2.4. Computational Methodology

All calculations were carried out using the Gaussian 09 suite of programs (version E.01) [32]. The geometries of all studied complexes were optimized using the M06-2x/aug-cc-pVDZ theoretical level [33,34], with frequency calculations conducted at the same level. Furthermore, the atoms-in-molecules (AIM) analysis [35] and atomic-dipole-moment-corrected Hirshfeld (ADCH) charge [36] calculations were performed using the Multiwfn program (version 3.8) [37], which were then visualized using the VMD package [38].

3. Results and Discussion

Figure 1 presents the CO_2 uptake by [TMGH][4-F-PhO] and [TMGH][4-F-PhO]-EG used in this work. As can be seen in Figure 1, the CO_2 capacity of [TMGH][4-F-PhO] is low (0.096 mol CO_2/mol IL) at 25 °C and 1.0 atm. The CO_2 capacity of EG is low as well (0.01 mol CO_2/mol EG) in the same conditions (Supplementary Material Figure S1). Based on the CO_2 capacities of [TMGH][4-F-PhO] and EG, it is reasonable to assume that the capacity of [TMGH][4-F-PhO]-EG will be similar to that of [TMGH][4-F-PhO]. Unexpectedly, the CO_2 capacity of [TMGH][4-F-PhO]-EG is much higher than that of [TMGH][4-F-PhO]. The solvents [TMGH][4-F-PhO]:EG (1:2, molar ratio), (1:3), and (1:4) can absorb 0.97, 0.98, and 0.98 mol CO_2/mol IL, respectively. It should be noted that the viscosity of [TMGH][4-F-PhO] is low at 25 °C (106 mPa·s), and the change in the viscosity of [TMGH][4-F-PhO] after uptake is not obvious. Therefore, the impact of the viscosity on the capacity can be neglected. The [TMGH][Car]-based systems show similar phenomena (Figure S2). [TMGH][Car] could absorb 0.097 mol CO_2/mol IL. [TMGH][Car]:EG (1:2), (1:3), and (1:4) could absorb 0.99, 1.01, and 1.03 mol CO_2/mol IL, respectively. The viscosity of [TMGH][Car] is as low as 58 mPa·s at 25 °C, and the change in the viscosity of [TMGH][Car] after uptake is not obvious as well. The capacity of $[N_{4444}]$Cl:EG(1:2)($[N_{4444}]$Cl: tetrabutylammonium chloride) is also measured, which is much lower (0.07 mol CO_2/mol IL) than that of [TMGH][4-F-PhO]:EG (1:2) (0.97 mol CO_2/mol IL) (Figure S1). The comparison of CO_2 capacities by the solvents used in this work with other IL-based solvents is shown in Table S1. With the aim of clarifying the unusual absorption behaviors of the sorbents used, NMR, FTIR, and theoretical calculations are used to investigate intermolecular interactions.

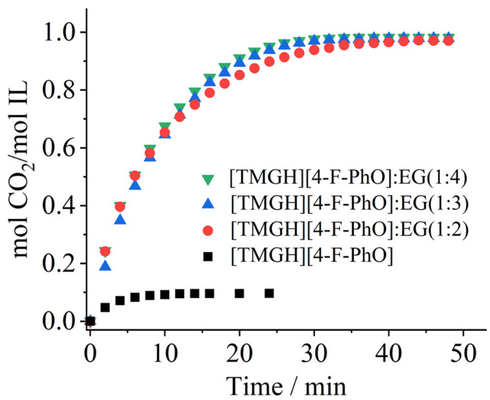

Figure 1. CO_2 uptake by [TMGH][4-F-PhO]-EG and [TMGH][4-F-PhO] at 25 °C and 1.0 atm.

The NMR (^{1}H and ^{13}C) spectra of [TMGH][4-F-PhO]:EG (1:3) with and without CO_2 are presented in Figure 2. There are two new proton signals at 3.48 (H-2) and 3.78 (H-3) ppm after CO_2 capture in the ^{1}H NMR spectra (Figure 2a), and three new carbon signals at 61.1 (C-2), 66.0 (C-3), and 157.3 (C-4) ppm can be found after capture in the ^{13}C NMR spectra (Figure 2b). The above-mentioned new peaks suggest that CO_2 reacts with EG in the solvent, forming EG-derived carbonate [39,40]. The peak at 157.3 (C-4) ppm is attributed to the carbonyl carbon of the carbonate species produced from the reaction between CO_2 and EG [41]. For the [TMGH][Car]:EG (1:3) system, similar new hydrogen and carbon peaks can be detected as well in the NMR spectra after capture (Figure S3).

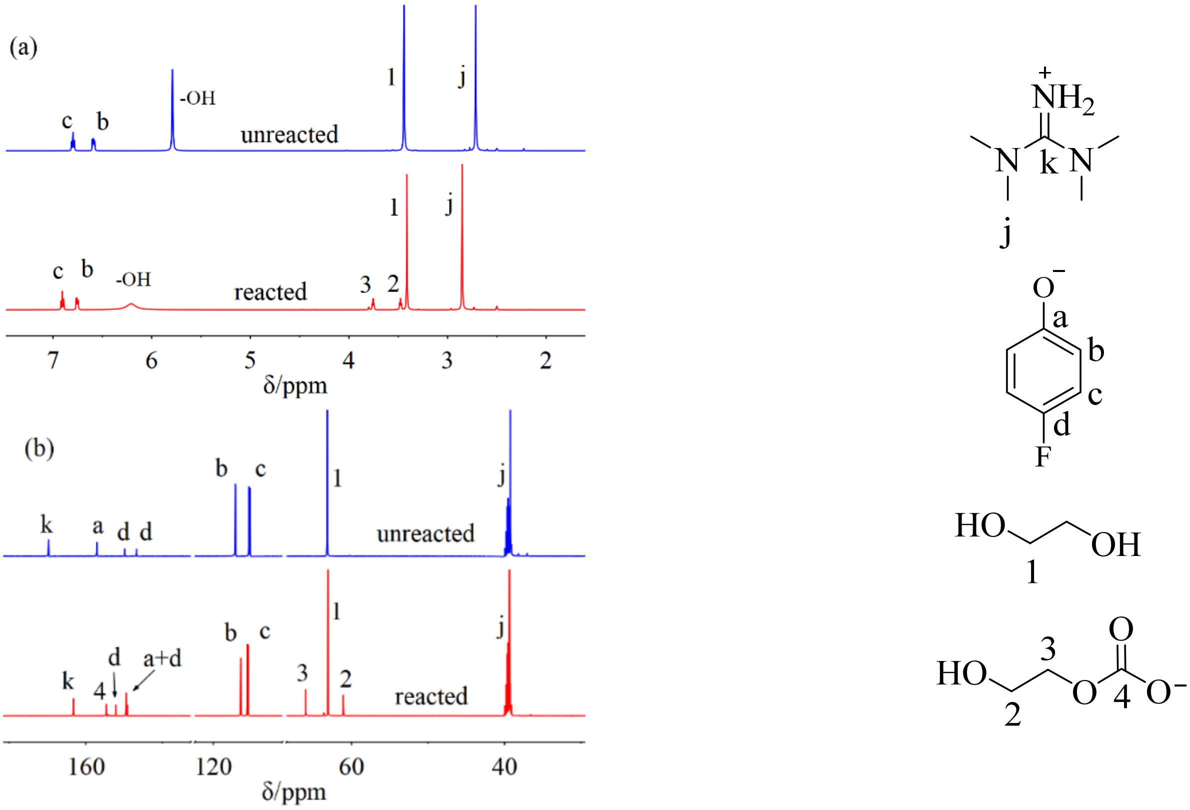

Figure 2. The ^{1}H (**a**) and ^{13}C (**b**) NMR spectra of [TMGH][4−F−PhO]:EG (1:3) with and without CO_2.

The NMR spectra of [TMGH][4-F-PhO] with and without CO_2 are presented in Figure 3. In the ^{1}H NMR spectra, the changes in the chemical shift in [TMGH][4-F-PhO]-based peaks are not obvious and no new peaks can be detected after capture. No new peaks can be found as well after capture in the ^{13}C NMR spectra. The NMR results indicate that the reaction between [TMGH][4-F-PhO] and CO_2 can be neglected. Similarly, the NMR spectra of [TMGH][Car] before and after CO_2 also reveal that CO_2 does not react with [TMGH][Car] (Figure S4).

The interactions between solvents and CO_2 are also disclosed using FTIR spectra. As shown in Figure 4a, there are two new peaks located at 1634 and 1289 cm^{-1} after CO_2 uptake for the [TMGH][4-F-PhO]:EG (1:3) absorbent. The band at 1634 cm^{-1} is assigned to the C=O stretching mode of $OCOO^-$, and the band centered at 1289 cm^{-1} can be due to the O-C-O stretching mode [39]. The FTIR results suggest the formation of carbonate species after absorption. Similar bands can be found as well in the FTIR spectra of [TMGH][4-F-PhO]:EG (1:2) and (1:4) after CO_2 capture. For the [TMGH][Car]:EG (1:3) solvent, new bands centered at 1638 and 1288 cm^{-1} are observed after CO_2 uptake (Figure S5a). However, in the spectra of [TMGH][4-F-PhO] after CO_2 capture (Figure 4b), no new bands can be observed, indicating that the chemical interactions between [TMGH][4-F-PhO] and CO_2

can be neglected. Similar to [TMGH][4-F-PhO], in the FTIR spectra of the [TMGH][Car] system, no new bands can be observed as well after capture (Figure S5b).

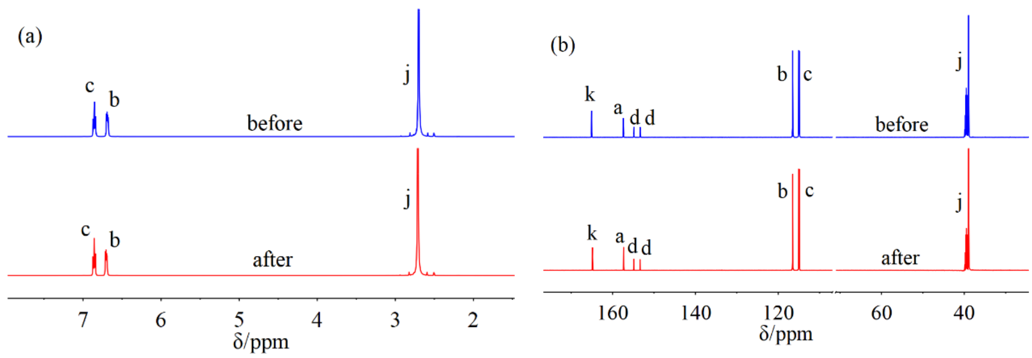

Figure 3. The ^{1}H (**a**) and ^{13}C (**b**) NMR spectra of [TMGH][4-F-PhO] with and without CO_2.

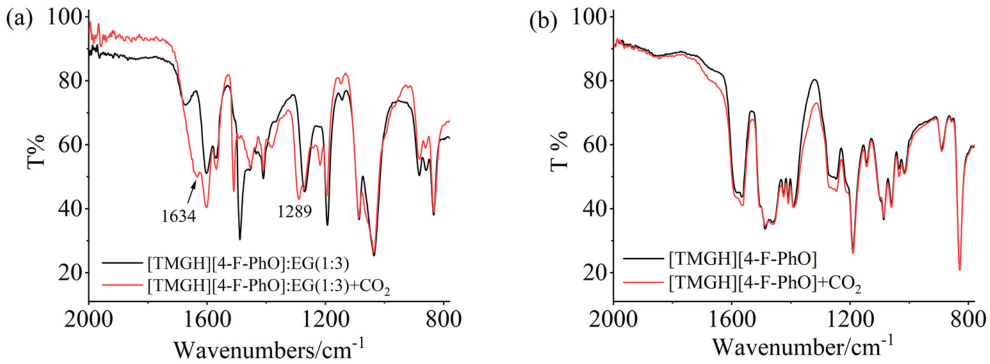

Figure 4. The FTIR spectra of [TMGH][4−F−PhO]:EG (1:3) (**a**) and [TMGH][4−F−PhO] (**b**) before and after absorption.

The possible carbon capture mechanisms by [TMGH][4-F-PhO]:EG (1:3) or [TMGH][Car]:EG (1:3) can be proposed according to the results discussed above. Scheme 1 shows the reaction mechanism between [TMGH][4-F-PhO]:EG (1:3) and CO_2. In the [TMGH][4-F-PhO]:EG (1:3), the anion [4-F-PhO]$^{-}$ can deprotonate EG, forming the anion HO-CH_2-CH_2-O^{-}. When CO_2 is bubbled into [TMGH][4-F-PhO]:EG (1:3), the base HO-CH_2-CH_2-O^{-} can attack CO_2, resulting in the formation of a carbonate species derived from EG. The capture mechanism of [TMGH][Car]-EG is similar to that of [TMGH][4-F-PhO]-EG.

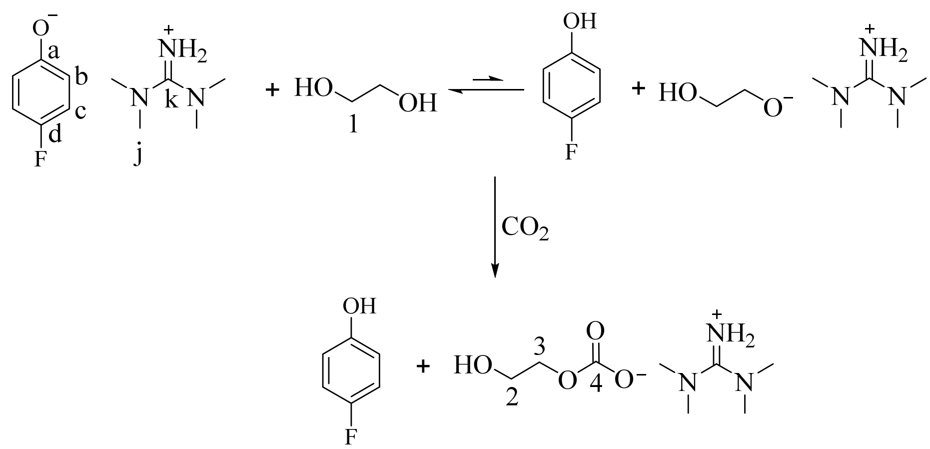

Scheme 1. The possible reaction mechanism between CO_2 and [TMGH][4−F−PhO]−EG solvents used in this work.

Considering the above-mentioned findings, the possible reason for the unusual CO_2 capture behaviors can be obtained. The pK_a values of EG, $[TMGH]^+$, and 4-F-PhOH are 15.1 [42], 13.0 [43], and 9.9 [44], respectively. $[TMGH]^+$ is therefore a stronger acid and a stronger hydrogen bond donor in comparison to EG. The strength of ionic hydrogen bonds (IHBs) can be estimated using ΔpK_a, which is the difference between the pK_a values of hydrogen bond donors and the conjugated acid of bond acceptors. The hydrogen bond strength will increase with decreasing ΔpK_a values [45,46]. Therefore, the hydrogen bond strength between $[TMGH]^+$ and $[4\text{-F-PhO}]^-$ (ΔpK_a = 3.1) is stronger than that between EG and the anion $[4\text{-F-PhO}]^-$ (ΔpK_a = 5.2). The strong hydrogen bonds formed between $[TMGH]^+$ and $[4\text{-F-PhO}]^-$ may cause IL [TMGH][4-F-PhO] to be chemically inert to CO_2. As EG is introduced into [TMGH][4-F-PhO], EG will create hydrogen bonds with $[4\text{-F-PhO}]^-$. In other words, EG will compete with $[TMGH]^+$ in the solvents. The competition between EG and $[TMGH]^+$ will reduce the hydrogen bond strength between $[TMGH]^+$ and $[4\text{-F-PhO}]^-$. The weakened hydrogen bond between $[TMGH]^+$ and $[4\text{-F-PhO}]^-$ may increase the basicity of $[4\text{-F-PhO}]^-$, so [TMGH][4-F-PhO]-EG systems are chemically active to CO_2.

The hydrogen bonding interactions between $[4\text{-F-PhO}]^-$ and EG are confirmed by ^{1}H NMR spectra (Figure 5a). The -OH proton of EG is at 4.54 ppm, and it shifts downfield to 5.79 ppm after EG is mixed with [TMGH][4-F-PhO], suggesting the creation of hydrogen bonds between the -OH proton and $[4\text{-F-PhO}]^-$. The hydrogen on the benzene ring moves upfield from 6.69 ppm (H-b) for [TMGH][4-F-PhO] to 6.59 ppm (H-b) for [TMGH][4-F-PhO]:EG (1:3), and the H-c signal also shifts upfield. Furthermore, the signal of the C-a carbon moves downfield from 157.4 ppm in [TMGH][4-F-PhO] to 158.6 ppm in [TMGH][4-F-PhO]:EG (1:3) (Figure 5b). The changes in the aforementioned carbon and hydrogen signals indicate that the introduction of EG into [TMGH][4-F-PhO] weakens the hydrogen bond strength between $[TMGH]^+$ and $[4\text{-F-PhO}]^-$, which causes the redistribution of the electron densities of related atoms on the benzene ring.

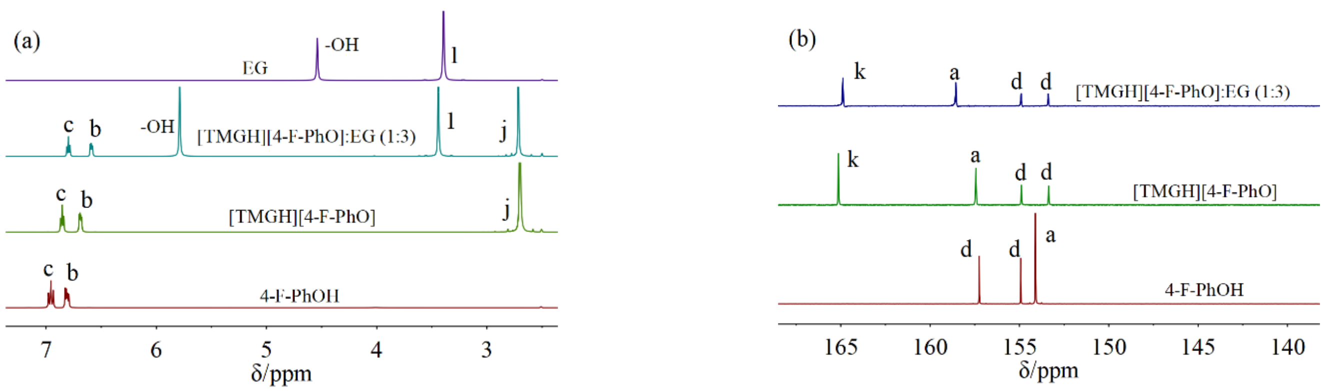

Figure 5. (**a**) The ^{1}H NMR spectra of EG, [TMGH][4-F-PhO]:EG (1:3), [TMGH][4-F-PhO], and 4-F-PhOH; (**b**) ^{13}C NMR spectra of [TMGH][4-F-PhO]:EG (1:3), [TMGH][4-F-PhO], and 4-F-PhOH.

Theoretical calculations are also used to gain further insights into the hydrogen bonds between EG and [TMGH][4-F-PhO]. The electrostatic potential (ESP) profiles of the anion $[4\text{-F-PhO}]^-$, the cation $[TMGH]^+$, and EG molecules upon their molecular surfaces are computed and depicted. Given that the dominant impetus behind the formation of attractive forces between these systems arises from their electrostatic interactions, this approach offers profound insights. Consequently, we mapped the ESP of the cation, anion, and EG on the van der Waals surface, as shown in Figure 6.

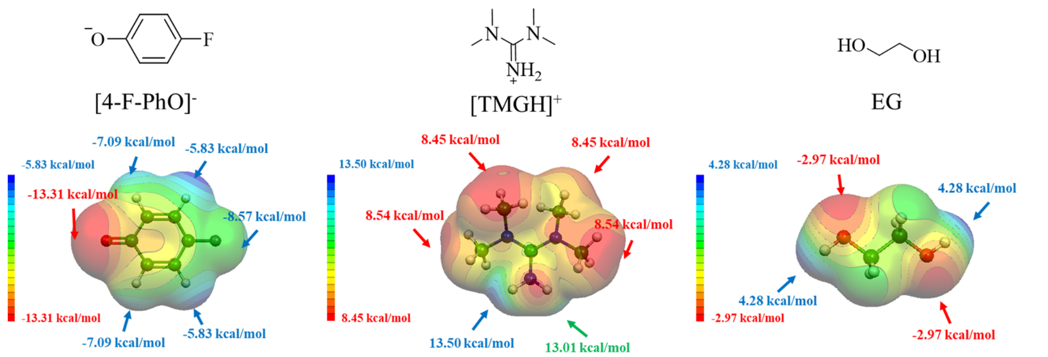

Figure 6. The ESP on the vdW surface (isosurface = 0.001 a.u.) of anion $[4-F-PhO]^-$, cation $[TMGH]^+$, and $V_{s,max}$ and $V_{s,min}$ for ions and molecules.

In the case of the anion $[4\text{-F-PhO}]^-$, the region of most negativity (−13.31 kcal/mol) manifests itself proximal to the oxygen atom, which can attributed to the presence of lone pair electrons. For the cation $[TMGH]^+$, the regions of highest positivity are situated at the periphery of the hydrogen atoms within the amino group. This observation indicates a propensity for the establishment of robust hydrogen bonds, potentially involving the N-H covalent bond. As for the EG molecule, the oxygen atoms of hydroxyl groups exhibit the most substantial ESP values (−2.97 kcal/mol) due to the existence of lone pair electrons. Consequently, these O atoms are appropriate candidates for hydrogen bond acceptors. Conversely, the hydrogen atoms of hydroxyl groups show the most positive ESP value (+4.28 kcal/mol), rendering them appropriate candidates for hydrogen bond donors.

The atoms-in-molecules (AIM) analysis is employed to study hydrogen bond interactions. The AIM analysis, which relies on the identification of critical points (CPs) situated between neighboring atoms, effectively discerns and confirms the presence of the crucial interactions. Notably, an AIM analysis of all hydrogen bonds in the investigated systems results in the identification of CPs between the atoms involved, as illustrated in Figure 7 and Table 1. The corresponding hydrogen bond energies (E_{HB}) can be obtained from the potential energy density (V) at the CPs [47]. For [TMGH][4-F-PhO] IL, the N-H···O and C-H···O hydrogen bonds are formed between $[TMGH]^+$ and $[4\text{-F-PhO}]^-$. The hydrogen bond energy of the N-H···O hydrogen bond (−21.0 kcal/mol) is far larger (absolute value) than that of the C-H···O bond (−3.3 kcal/mol), indicating that the hydrogen bond between the amine proton on the cation and the O atom on the anion is much stronger than that between the methyl proton on the cation and the O atom on the anion in [TMGH][4-F-PhO] [48]. As expected, the N-H···O bond length (1.576Å) is much shorter than that of the C-H···O bond (2.385 Å). The strong N-H···O hydrogen bond may make [TMGH][4-F-PhO] unreactive to CO_2.

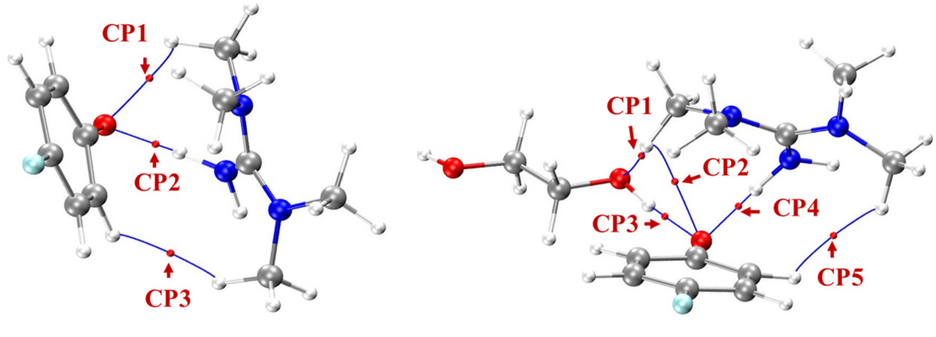

[TMGH][4-F-PhO] [TMGH][4-F-PhO]-EG

Figure 7. The hydrogen bonds in [TMGH][4-F-PhO] and [TMGH][4-F-PhO]-EG.

Table 1. The geometric and energetic data for the hydrogen bonds studied.

Systems	[a] CP	HB	[b] d_{HB}	[c] $angle_{HB}$	[d] E_{HB}
[TMGH][4-F-PhO]	CP1	C-H···O	2.385	117.7	−3.3
	CP2	N-H···O	1.576	161.5	−21.0
	CP3	C-H···H-C	2.304	137.9	−1.0
[TMGH][4-F-PhO]-EG	CP1	C-H···O	2.637	109.2	−2.0
	CP2	C-H···O	2.560	109.9	−2.6
	CP3	O-H···O	1.677	172.8	−13.1
	CP4	N-H···O	1.620	161.1	−17.6
	CP5	C-H···H-C	2.394	137.6	−0.8

[a] critical points of hydrogen bonds; [b] bond length in Å; [c] bond angles in degrees; [d] bond energies in kcal/mol.

In the binary system [TMGH] [4-F-PhO]-EG, a complex network of hydrogen bonds is established. After the addition of EG into [TMGH] [4-F-PhO], the N-H···O bond strength between $[TMGH]^+$ and $[4\text{-F-PhO}]^-$ becomes weaker (−17.6 kcal/mol) compared with that (−21.0 kcal/mol) in pure [TMGH] [4-F-PhO]. The N-H···O bond length also becomes longer from 1.576 Å in [TMGH] [4-F-PhO] to 1.620 Å in [TMGH] [4-F-PhO]-EG. Moreover, the O-H···O hydrogen bond is also created between the proton of the -OH group and the O atom of the $[4\text{-F-PhO}]^-$ anion, and this O-H···O hydrogen bond length is 1.677 Å. The calculated results above reveal that EG indeed competes with $[TMGH]^+$ to form hydrogen bonds with $[4\text{-F-PhO}]^-$, and this competition therefore reduces the N-H···O bond strength. The above discussion presents an agreement between the theoretical results and experimental data.

The interactions between CO_2 and [TMGH] [4-F-PhO] or [TMGH] [4-F-PhO]-EG are also investigated through theoretical calculations (Figure 8). The enthalpy change (ΔH) for [TMGH] [4-F-PhO] + CO_2 is −7.4 kcal/mol. However, the ΔH value for [TMGH] [4-F-PhO]-EG + CO_2 is −15.8 kcal/mol. In other words, the interaction between CO_2 and [TMGH] [4-F-PhO]-EG is much stronger than that between CO_2 and [TMGH] [4-F-PhO], which is in agreement with the experimental results.

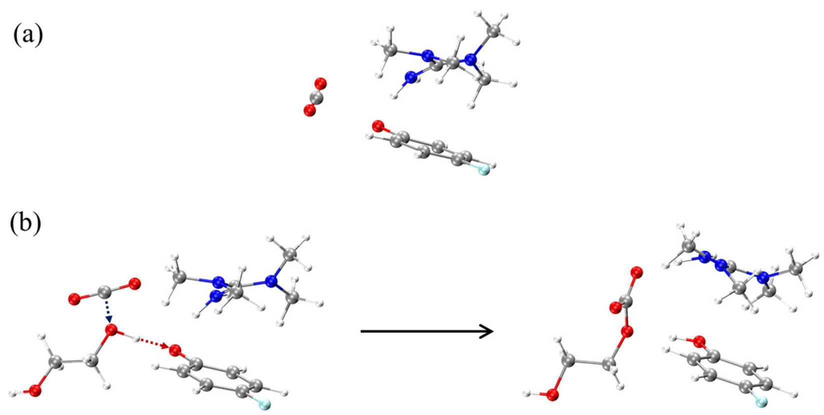

Figure 8. The interactions between CO_2 and absorbents: (**a**) [TMGH][4-F-PhO] + CO_2; (**b**) [TMGH][4-F-PhO]-EG + CO_2.

The reusability of [TMGH] [4-F-PhO]:EG (1:2) is also studied. The absorbed CO_2 can be released by blowing N_2 onto the absorbent at 70 °C, and [TMGH] [4-F-PhO]:EG (1:2) can be reused (Figure S6). The DSC curves of [TMGH] [4-F-PhO]-EG and [TMGH] [4-F-PhO] are shown in Figure S7. The melting points of [TMGH] [4-F-PhO]:EG (1:2), (1:3), and (1:4) are −62.6, −74.2, and −81.8 °C, respectively. These melting points are lower than those of [TMGH][4-F-PhO] (−48.2 °C) and EG (−11.5 °C) [39], suggesting that the solvents formed by EG and protic ionic liquid [TMGH][4-F-PhO] can be classified as deep eutectic solvents [28,39].

4. Conclusions

In summary, TMG-based ILs ([TMGH][4-F-PhO] and [TMGH][Car]) and Ils-EG mixtures are studied for CO_2 capture. The NMR and FTIR results indicate that the TMG-based ILs studied in this work are chemically inert to CO_2. Nevertheless, after mixing ILs with EG, the formed ILs-EG mixtures can chemically capture CO_2, thus resulting in the higher CO_2 capacities of ILs-EG absorbents than those of ILs. The NMR and theoretical calculation studies provide insights into the CO_2 absorption behaviors, and the hydrogen bonds play an important role in tuning the CO_2 absorption process. The strong hydrogen bonds between $[TMGH]^+$ and phenolate anions are responsible for the ILs' nonreactivity to CO_2. The hydrogen bonds from EG weaken the bond between $[TMGH]^+$ and phenolate anions, which causes ILs-EG solvents to be able to chemically capture CO_2.

Supplementary Materials: The following supporting information can be downloaded at https://www.mdpi.com/article/10.3390/atmos15020229/s1. Figure S1: CO_2 absorption by EG and $[N_{4444}]$Cl:EG (1:2) at 25 °C and 1.0 atm; Figure S2: CO_2 absorption by [TMGH][Car] and [TMGH][Car]-EG at 25 °C and 1.0 atm; Table S1: Comparison of CO_2 capacities in this work with other IL-based solvents ([49–58]); Figure S3: The ^{1}H (a) and ^{13}C (b) NMR spectra of [TMGH][Car]:EG (1:3) before and after absorption; Figure S4: The ^{1}H (a) and ^{13}C (b) NMR spectra of [TMGH][Car] before and after absorption; Figure S5: The FTIR spectra of [TMGH][Car]:EG (1:3) (a) and [TMGH][Car] (b) before and after absorption. Figure S6: The absorption–desorption cycles of [TMGH][4-F-PhO]:EG (1:2): absorption, 20 °C; desorption, 70 °C; Figure S7: The DSC curves of [TMGH][4-F-PhO]-EG and [TMGH][4-F-PhO].

Author Contributions: Conceptualization, D.Y.; methodology, B.L., Y.Z., S.Z. and D.Y.; investigation, B.L., Y.Z., M.C., S.Z. and D.Y.; data curation, B.L., Y.Z. and M.C.; writing—original draft preparation, B.L. and Y.Z.; writing—review and editing, S.Z. and D.Y.; supervision, S.Z. and D.Y.; funding acquisition, S.Z. and D.Y. All authors have read and agreed to the published version of the manuscript.

Funding: This research was funded by the Fundamental Research Funds for the Central Universities, grant number 2652019111; the National Natural Science Foundation of China, grant number 22108111; the Natural Science Foundation of Yunnan Province, grant number 202101AU070021; the Natural Science Foundation of Kunming University of Science and Technology, grant number KKZ3202052038; and the Xingdian Talent Support Project, grant number YNQR-QNRC-2020-081.

Data Availability Statement: Data that support the findings of this study are available from the corresponding author upon reasonable request.

Conflicts of Interest: The authors declare no conflicts of interest.

References

1. Zhang, Z.; Zheng, Y.; Qian, L.; Luo, D.; Dou, H.; Wen, G.; Yu, A.; Chen, Z. Emerging Trends in Sustainable CO_2-Management Materials. *Adv. Mater.* **2022**, *34*, 2201547. [CrossRef] [PubMed]
2. Madejski, P.; Chmiel, K.; Subramanian, N.; Kuś, T. Methods and Techniques for CO_2 Capture: Review of Potential Solutions and Applications in Modern Energy Technologies. *Energies* **2022**, *15*, 887. [CrossRef]
3. Aghel, B.; Janati, S.; Wongwises, S.; Shadloo, M.S. Review on CO_2 capture by blended amine solutions. *Int. J. Greenh. Gas Control* **2022**, *119*, 103715. [CrossRef]
4. Sun, S.; Sun, H.; Williams, P.T.; Wu, C. Recent advances in integrated CO_2 capture and utilization: A review. *Sustain. Energy Fuels* **2021**, *5*, 4546–4559. [CrossRef]
5. Wang, Y.; He, H.; Wang, C.; Lu, Y.; Dong, K.; Huo, F.; Zhang, S. Insights into Ionic Liquids: From Z-Bonds to Quasi-Liquids. *JACS Au* **2022**, *2*, 543–561. [CrossRef] [PubMed]
6. Kaur, G.; Kumar, H.; Singla, M. Diverse applications of ionic liquids: A comprehensive review. *J. Mol. Liq.* **2022**, *351*, 118556. [CrossRef]
7. Pei, Y.; Zhang, Y.; Ma, J.; Fan, M.; Zhang, S.; Wang, J. Ionic liquids for advanced materials. *Mater. Today Nano* **2022**, *17*, 100159. [CrossRef]
8. Piatti, E.; Guglielmero, L.; Tofani, G.; Mezzetta, A.; Guazzelli, L.; D'Andrea, F.; Roddaro, S.; Pomelli, C.S. Ionic liquids for electrochemical applications: Correlation between molecular structure and electrochemical stability window. *J. Mol. Liq.* **2022**, *364*, 120001. [CrossRef]
9. Zhang, R.; Ke, Q.; Zhang, Z.; Zhou, B.; Cui, G.; Lu, H. Tuning Functionalized Ionic Liquids for CO_2 Capture. *Int. J. Mol. Sci.* **2022**, *23*, 11401. [CrossRef]

10. Suo, X.; Fu, Y.; Do-Thanh, C.-L.; Qiu, L.-Q.; Jiang, D.-e.; Mahurin, S.M.; Yang, Z.; Dai, S. CO_2 Chemisorption Behavior in Conjugated Carbanion-Derived Ionic Liquids via Carboxylic Acid Formation. *J. Am. Chem. Soc.* **2022**, *144*, 21658–21663. [CrossRef] [PubMed]
11. Qiu, L.; Fu, Y.; Yang, Z.; Johnson, A.C.; Do-Thanh, C.-L.; Thapaliya, B.P.; Mahurin, S.M.; He, L.-N.; Jiang, D.-E.; Dai, S. Surpassing the Performance of Phenolate-derived Ionic Liquids in CO_2 Chemisorption by Harnessing the Robust Nature of Pyrazolonates. *ChemSusChem* **2023**, e202301329. [CrossRef] [PubMed]
12. Yoon, B.; Voth, G.A. Elucidating the Molecular Mechanism of CO_2 Capture by Amino Acid Ionic Liquids. *J. Am. Chem. Soc.* **2023**, *145*, 15663–15667. [CrossRef] [PubMed]
13. Gurau, G.; Rodríguez, H.; Kelley, S.P.; Janiczek, P.; Kalb, R.S.; Rogers, R.D. Demonstration of Chemisorption of Carbon Dioxide in 1,3-Dialkylimidazolium Acetate Ionic Liquids. *Angew. Chem. Int. Ed.* **2011**, *50*, 12024–12026. [CrossRef] [PubMed]
14. Wang, C.; Luo, X.; Luo, H.; Jiang, D.-e.; Li, H.; Dai, S. Tuning the Basicity of Ionic Liquids for Equimolar CO_2 Capture. *Angew. Chem. Int. Ed.* **2011**, *50*, 4918–4922. [CrossRef]
15. Seo, S.; Quiroz-Guzman, M.; DeSilva, M.A.; Lee, T.B.; Huang, Y.; Goodrich, B.F.; Schneider, W.F.; Brennecke, J.F. Chemically Tunable Ionic Liquids with Aprotic Heterocyclic Anion (AHA) for CO_2 Capture. *J. Phys. Chem. B* **2014**, *118*, 5740–5751. [CrossRef]
16. Seo, S.; DeSilva, M.A.; Xia, H.; Brennecke, J.F. Effect of Cation on Physical Properties and CO_2 Solubility for Phosphonium-Based Ionic Liquids with 2-Cyanopyrrolide Anions. *J. Phys. Chem. B* **2015**, *119*, 11807–11814. [CrossRef]
17. Wang, C.; Luo, H.; Li, H.; Zhu, X.; Yu, B.; Dai, S. Tuning the Physicochemical Properties of Diverse Phenolic Ionic Liquids for Equimolar CO_2 Capture by the Substituent on the Anion. *Chem. Eur. J.* **2012**, *18*, 2153–2160. [CrossRef]
18. Luo, X.; Guo, Y.; Ding, F.; Zhao, H.; Cui, G.; Li, H.; Wang, C. Significant Improvements in CO_2 Capture by Pyridine-Containing Anion-Functionalized Ionic Liquids through Multiple-Site Cooperative Interactions. *Angew. Chem. Int. Ed.* **2014**, *53*, 7053–7057. [CrossRef]
19. Huang, Y.; Cui, G.; Zhao, Y.; Wang, H.; Li, Z.; Dai, S.; Wang, J. Preorganization and Cooperation for Highly Efficient and Reversible Capture of Low-Concentration CO_2 by Ionic Liquids. *Angew. Chem. Int. Ed.* **2017**, *56*, 13293–13297. [CrossRef]
20. Wang, C.; Luo, H.; Jiang, D.-e.; Li, H.; Dai, S. Carbon Dioxide Capture by Superbase-Derived Protic Ionic Liquids. *Angew. Chem. Int. Ed.* **2010**, *49*, 5978–5981. [CrossRef]
21. Lei, X.; Xu, Y.; Zhu, L.; Wang, X. Highly efficient and reversible CO_2 capture through 1,1,3,3-tetramethylguanidinium imidazole ionic liquid. *Rsc. Adv.* **2014**, *4*, 7052–7057. [CrossRef]
22. Zhu, X.; Song, M.; Xu, Y. DBU-Based Protic Ionic Liquids for CO_2 Capture. *ACS Sustain. Chem. Eng.* **2017**, *5*, 8192–8198. [CrossRef]
23. Gao, F.; Wang, Z.; Ji, P.; Cheng, J.-P. CO_2 Absorption by DBU-Based Protic Ionic Liquids: Basicity of Anion Dictates the Absorption Capacity and Mechanism. *Front. Chem.* **2019**, *6*, 658. [CrossRef] [PubMed]
24. Li, F.; Bai, Y.; Zeng, S.; Liang, X.; Wang, H.; Huo, F.; Zhang, X. Protic ionic liquids with low viscosity for efficient and reversible capture of carbon dioxide. *Int. J. Greenh. Gas Control* **2019**, *90*, 102801. [CrossRef]
25. Oncsik, T.; Vijayaraghavan, R.; MacFarlane, D.R. High CO_2 absorption by diamino protic ionic liquids using azolide anions. *Chem. Commun.* **2018**, *54*, 2106–2109. [CrossRef] [PubMed]
26. Simons, T.J.; Verheyen, T.; Izgorodina, E.I.; Vijayaraghavan, R.; Young, S.; Pearson, A.K.; Pas, S.J.; MacFarlane, D.R. Mechanisms of low temperature capture and regeneration of CO_2 using diamino protic ionic liquids. *Phys. Chem. Chem. Phys.* **2016**, *18*, 1140–1149. [CrossRef]
27. Wang, X.; Wu, C.; Yang, D. CO_2 Absorption Mechanism by Diamino Protic Ionic Liquids (DPILs) Containing Azolide Anions. *Processes* **2021**, *9*, 1023. [CrossRef]
28. Mukesh, C.; Khokarale, S.G.; Virtanen, P.; Mikkola, J.-P. Rapid desorption of CO_2 from deep eutectic solvents based on polyamines at lower temperatures: An alternative technology with industrial potential. *Sustain. Energy Fuels* **2019**, *3*, 2125–2134. [CrossRef]
29. Xiong, W.; Shi, M.; Peng, L.; Zhang, X.; Hu, X.; Wu, Y. Low viscosity superbase protic ionic liquids for the highly efficient simultaneous removal of H_2S and CO_2 from CH_4. *Sep. Purif. Technol.* **2021**, *263*, 118417. [CrossRef]
30. Zailani, N.H.Z.O.; Yunus, N.M.; Ab Rahim, A.H.; Bustam, M.A. Experimental Investigation on Thermophysical Properties of Ammonium-Based Protic Ionic Liquids and Their Potential Ability towards CO_2 Capture. *Molecules* **2022**, *27*, 851. [CrossRef]
31. Ma, J.; Wang, Y.; Yang, X.; Zhu, M.; Wang, B. DFT Study on the Chemical Absorption Mechanism of CO_2 in Diamino Protic Ionic Liquids. *J. Phys. Chem. B* **2021**, *125*, 1416–1428. [CrossRef]
32. Frisch, M.T.; Trucks, G.W.; Schlegel, H.B.; Scuseria, G.; Robb, M.; Cheeseman, J.; Scalmani, G.; Barone, V.; Mennucci, B.; Petersson, G. *Gaussian 09, Revision D. 01*; Gaussian, Inc.: Wallingford, CT, USA, 2009.
33. Zhao, Y.; Truhlar, D.G. The M06 suite of density functionals for main group thermochemistry, thermochemical kinetics, noncovalent interactions, excited states, and transition elements: Two new functionals and systematic testing of four M06-class functionals and 12 other functionals. *Theor. Chem. Acc.* **2008**, *120*, 215–241.
34. Kendall, R.A.; Dunning, T.H.; Harrison, R.J., Jr. Electron affinities of the first—Row atoms revisited. Systematic basis sets and wave functions. *J. Chem. Phys.* **1992**, *96*, 6796–6806. [CrossRef]
35. Bader, R.F.W. Atoms in molecules. *Acc. Chem. Res.* **1985**, *18*, 9–15. [CrossRef]
36. Lu, T.; Chen, F. Atomic dipole moment corrected hirshfeld population method. *J. Theor. Comput. Chem.* **2012**, *11*, 163. [CrossRef]
37. Lu, T.; Chen, F. Multiwfn: A multifunctional wavefunction analyzer. *J. Comput. Chem.* **2012**, *33*, 580–592. [CrossRef]
38. Humphrey, W.; Dalke, A.; Schulten, K. VMD: Visual molecular dynamics. *J. Mol. Graph. Model.* **1996**, *14*, 33–38. [CrossRef] [PubMed]

39. Lee, Y.-Y.; Penley, D.; Klemm, A.; Dean, W.; Gurkan, B. Deep Eutectic Solvent Formed by Imidazolium Cyanopyrrolide and Ethylene Glycol for Reactive CO_2 Separations. *ACS Sustain. Chem. Eng.* **2021**, *9*, 1090–1098. [CrossRef]
40. Wang, Z.; Wu, C.; Wang, Z.; Zhang, S.; Yang, D. CO_2 capture by 1,2,3-triazole-based deep eutectic solvents: The unexpected role of hydrogen bonds. *Chem. Commun.* **2022**, *58*, 7376–7379. [CrossRef]
41. Chen, M.; Xu, J. CO_2 Capture Mechanism by Deep Eutectic Solvents Formed by Choline Prolinate and Ethylene Glycol. *Molecules* **2023**, *28*, 5461. [CrossRef]
42. Ballinger, P.; Long, F.A. Acid Ionization Constants of Alcohols. II. Acidities of Some Substituted Methanols and Related Compounds. *J. Am. Chem. Soc.* **1960**, *82*, 795–798. [CrossRef]
43. Tshepelevitsh, S.; Kütt, A.; Lõkov, M.; Kaljurand, I.; Saame, J.; Heering, A.; Plieger, P.G.; Vianello, R.; Leito, I. On the Basicity of Organic Bases in Different Media. *Eur. J. Org. Chem.* **2019**, *2019*, 6735–6748. [CrossRef]
44. Bijloo, G.J.; Rekker, R.F. Some Critical Remarks Concerning the Inductive Parameter σI Part III: Parametrization of the Ortho Effect in Benzoic Acids and Phenols. *Quant. Struct. Act. Relatsh.* **1984**, *3*, 91–96. [CrossRef]
45. Gilli, P.; Pretto, L.; Bertolasi, V.; Gilli, G. Predicting Hydrogen-Bond Strengths from Acid−Base Molecular Properties. The pKa Slide Rule: Toward the Solution of a Long-Lasting Problem. *Acc. Chem. Res.* **2009**, *42*, 33–44. [CrossRef] [PubMed]
46. Grabowski, S.J. What is the Covalency of Hydrogen Bonding? *Chem. Rev.* **2011**, *111*, 2597–2625. [CrossRef] [PubMed]
47. Espinosa, E.; Molins, E.; Lecomte, C. Hydrogen bond strengths revealed by topological analyses of experimentally observed electron densities. *Chem. Phys. Lett.* **1998**, *285*, 170–173. [CrossRef]
48. Aquino, A.J.A.; Tunega, D.; Haberhauer, G.; Gerzabek, M.H.; Lischka, H. Solvent Effects on Hydrogen Bonds: A Theoretical Study. *J. Phys. Chem. A* **2002**, *106*, 1862–1871. [CrossRef]
49. Zhang, N.; Huang, Z.; Zhang, H.; Ma, J.; Jiang, B.; Zhang, L. Highly Efficient and Reversible CO_2 Capture by Task-Specific Deep Eutectic Solvents. *Ind. Eng. Chem. Res.* **2019**, *58*, 13321–13329. [CrossRef]
50. Cui, G.; Lv, M.; Yang, D. Efficient CO_2 absorption by azolide-based deep eutectic solvents. *Chem. Commun.* **2019**, *55*, 1426–1429. [CrossRef] [PubMed]
51. Wang, Z.; Wang, Z.; Huang, X.; Yang, D.; Wu, C.; Chen, J. Deep eutectic solvents composed of bio-phenol-derived superbase ionic liquids and ethylene glycol for CO_2 capture. *Chem. Commun.* **2022**, *58*, 2160–2163. [CrossRef]
52. Wang, Z.; Wang, Z.; Chen, J.; Wu, C.; Yang, D. The Influence of Hydrogen Bond Donors on the CO_2 Absorption Mechanism by the Bio-Phenol-Based Deep Eutectic Solvents. *Molecules* **2021**, *26*, 7167. [CrossRef] [PubMed]
53. Fu, H.; Wang, X.; Sang, H.; Liu, J.; Lin, X.; Zhang, L. Highly efficient absorption of carbon dioxide by EG-assisted DBU-based deep eutectic solvents. *J. CO_2 Util.* **2021**, *43*, 101372. [CrossRef]
54. Nie, M.-N.; Wang, Z.; Niu, Q.-H.; Dai, J.-X.; Wang, Q.-Q.; Peng, J.-S.; Ji, P. Acidity Scale in a Choline Chloride- and Ethylene Glycol-Based Deep Eutectic Solvent and Its Implication on Carbon Dioxide Absorption. *J. Org. Chem.* **2023**, *88*, 5368–5376. [CrossRef] [PubMed]
55. Klemm, A.; Vicchio, S.P.; Bhattacharjee, S.; Cagli, E.; Park, Y.; Zeeshan, M.; Dikki, R.; Liu, H.; Kidder, M.K.; Getman, R.B.; et al. Impact of Hydrogen Bonds on CO_2 Binding in Eutectic Solvents: An Experimental and Computational Study toward Sorbent Design for CO_2 Capture. *ACS Sustain. Chem. Eng.* **2023**, *11*, 3740–3749. [CrossRef]
56. Jiang, B.; Ma, J.; Yang, N.; Huang, Z.; Zhang, N.; Tantai, X.; Sun, Y.; Zhang, L. Superbase/Acylamido-Based Deep Eutectic Solvents for Multiple-Site Efficient CO_2 Absorption. *Energy Fuels* **2019**, *33*, 7569–7577. [CrossRef]
57. Mei, K.; He, X.; Chen, K.; Zhou, X.; Li, H.; Wang, C. Highly Efficient CO_2 Capture by Imidazolium Ionic Liquids through a Reduction in the Formation of the Carbene–CO_2 Complex. *Ind. Eng. Chem. Res.* **2017**, *56*, 8066–8072. [CrossRef]
58. Luo, X.-Y.; Chen, X.-Y.; Qiu, R.-X.; Pei, B.-Y.; Wei, Y.; Hu, M.; Lin, J.-Q.; Zhang, J.-Y.; Luo, G.-G. Enhanced CO_2 capture by reducing cation–anion interactions in hydroxyl-pyridine anion-based ionic liquids. *Dalton Trans.* **2019**, *48*, 2300–2307. [CrossRef]